Replies to the reviews of our manuscript "First results from the GPS atmosphere sounding experiment TOR aboard the TerraSAR-X satellite"

We appreciate the effort and time that the reviewer has invested in our manuscript and thank him/her for his/her work.

Below we answer the reviewer's questions and describe the changes of the revised manuscript. The reviewer's comments are quoted in italics, our replies are indented and set in straight font.

Reviewer #1, comments for the Authors:

General Remarks:

Generally a well written article, with only a few minor things that should be clarified or amended. There is a large interest in obtaining radio occultation data in near real time for assimilation into numerical weather prediction models. Please add whether this is planned for TerraSAR-X (Tandem-X).

> Since 21 October 2010 GPSRO data from TerraSAR-X are provided to meteorological centers in real time. Data from IGOR aboard TanDEM-X will likewise be provided, once continuous GPSRO mode is activated on that spacecraft. In the revised manuscript (section 5 "Conclusions") the following sentence is added :
> "Since 21 October 2010 TerraSAR-X observations are included in GFZ's GPSRO operational processing system POCS and distributed via WMO's Global Telecommunications System to international meteorological centers (ECMWF, UK Met Office, Meteo France, NCEP, JMA und DWD)."

The focus is also shifted more to bending angles, thus a validation of these would greatly benefit the manuscript.

> We follow the reviewer's suggestion and add to section 4.4 ("Validation with ECMWF analyses") a discussion on bending angle validation. The comparison between observed bending angles (in the following denoted as α^{RO}) and ECMWF bending angles (α^{E}) as well as the procedures and algorithms employed in their derivation are described in the revised manuscript.
>
> The analysis of the GPSRO bending angles and the comparison with corresponding ECMWF bending angles revealed a number of outlier events. These profiles correlate with enhanced excess Doppler frequencies and were removed from the data set by reprocessing the complete data set with an additional criterion imposed on the excess Doppler. (Statistical optimization of the bending angles prevented these outliers to cause an appreciable degradation of the derived refractivities in the previous data version; see discussion below.) Furthermore, the filter order of the polynomial derivative filter used by the POCS-X processing system was increased from 61 to 101 (the value used by the POCS operational system) in order to improve the consistency between the two processing systems.
>
> The inverse Abel transform relates refractive index $n \equiv 1 + 10^{-6} \cdot N$ and bending angle α,
>
> $$\alpha(p) = -2\,p \int_{p}^{\infty} \frac{dx}{\sqrt{x^2 - p^2}} \, \frac{d\ln(n(x))}{dx} \ . \tag{1}$$

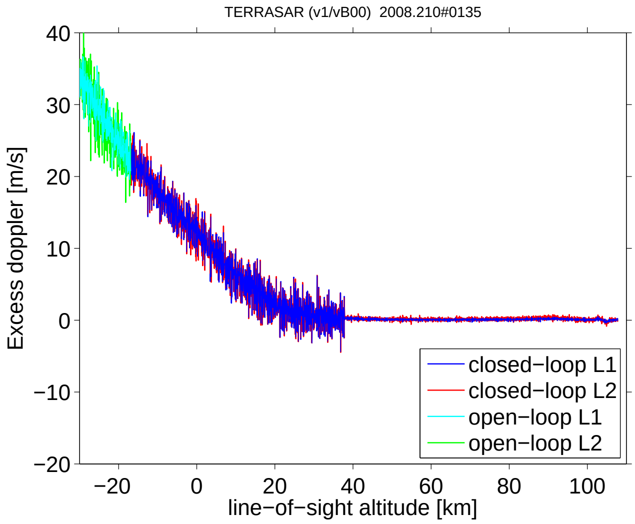

Figure 1: Excess doppler as a function of line-of-sight altitude derived from occultation event 135 on 28 July 2008 (2008.210#0135). At about 38 km line-of-sight altitude the standard deviation of the L1 and L2 Doppler (derivative of the excess phase path with respect to time) abruptly increases by about a factor of ten. This and similar observations are excluded from the data set by imposing the requirement that the modulus of the L1 and L2 Doppler remains below 4 m/s between 30 and 70 km line-of-sight altitude.

The Abel transform requires knowledge of the ECMWF refractivity profile (superscript E indicate ECMWF-derived profiles) $N^E \equiv 10^6 \cdot (n^E - 1)$ for altitudes up to about 120 km and vertical resolutions on the order of a few tens of meters. To reach that altitude, ECMWF profiles — ending at about 80 km — are extended (by extrapolation or an atmospheric model) and their vertical resolution is enhanced to 25 m by log-linear interpolation. Furthermore, POCS-X calculates refractivity profiles from the observed (superscript RO) bending angle profile $\alpha^{RO}(z)$ without adjusting its vertical resolution. which decreases from a corresponding step size of about 10 m in the troposphere to about 50 m in the stratosphere.

For the calculation of n the high-resolution (i.e. noisy) bending angle profile is used since the Abel transform

$$n^{RO}(r) = \exp\left(\frac{1}{\pi}\int_{p(r)}^{\infty}\frac{\alpha^{RO}(p')}{\sqrt{p^2 - p'^2}}dp'\right) \quad . \tag{2}$$

constitutes a low pass filter; i.e. the high frequency noise of $\alpha^{RO}(z)$ is suppressed and has little impact on the derived refractivity profile $N^{RO} \equiv 10^6 \cdot (n^{RO} - 1)$. The comparison between observed and ECMWF bending angle level profiles, on the other hand, necessitates compatibility of their respective vertical resolutions and therefore the vertical resolution of the high-resolution profiles $\alpha^{RO}(z)$ need to be reduced (see discussion below).

The comparison between observed and ECMWF bending angles uncovered a number of outlier events caused by strongly fluctuating excess Doppler noise; an example is shown in Fig. 1. It appears unlikely that these fluctuations originate from atmospheric or ionospheric phenomena; rather they appear to be related to instrumental effects. In order to remove these erroneous data the heuristic criteria

$$|dF_1/dt| < 4 \text{ m/s} \qquad \text{and} \qquad |dF_2/dt| < 4 \text{ m/s}$$

within line-of-sight altitudes between 30 and 70 km are imposed. Here, F_1 and F_2 denote the L1 and L2 excess phase path, respectively. In 244 out of 15,571 observed events (1.6%) one or both conditions are violated and the corresponding observation is removed. Modified versions of figures 5 and 10, as well as table 1 are included in revised manuscript (see below).

Section 4.4 ("Validation with ECMWF analyses") in the revised manuscript reads as follows:

"In this subsection the IGOR (TerraSAR-X) bending angle and refractivity profiles are compared with meteorological analysis results provided by the ECMWF. Pressure and temperature values at the time and location of the corresponding GPSRO measurement are calculated from the ECMWF fields using spatial and temporal linear interpolation between grid points ($0.5^o \times 0.5^o$ horizontal resolution) and analysis fields separated by 6 h. The vertical resolution of the GPSRO refractivity profiles is 100 m; the comparison between GPSRO observation and ECMWF data, however, is performed solely on the 91 ECMWF model levels ranging from the ground up to an altitude of about 80 km with a vertical resolution decreasing from about 25 m near the surface to about 500 m in the upper troposphere / lower stratosphere and to about 7 km at the upper model level. The comparison results, however, are not plotted as a function of the 91 ECMWF model level number, but as a function of the corresponding mean altitude.

In general, the bending angle profile $\alpha(p)$, corresponding a given refractivity profile N, follows from the inverse Abel transform (Fjeldbo et al., 1971; Hocke, 1997)

$$\alpha(p) = -2\,p \int_p^\infty \frac{dx}{\sqrt{x^2 - p^2}} \, \frac{d\ln(n(x))}{dx} \ . \tag{3}$$

Here, $n = 1 + 10^{-6}\,N$ denotes the real part of the refractive index and p is the impact parameter. Eqn. 3 is based on the assumption that the refractivity field is spherically symmetric, i.e. $N(\vec{r}) = N(r)$.

The bending angle profile α^E as a function of impact parameter p corresponding to a given ECMWF refractivity profile N^E is derived in the following way. First, on each of 91 model levels N^E is calculated from the corresponding ECMWF temperature, pressure and humidity data. Second, $N^E(z)$ is upsampled on an equidistant altitude grid with 25 m step size using log-linear interpolation. Third, $N^E(z)$ is extended from the upmost ECMWF altitude level (about 80 km) up to 120 km using log-linear extrapolation. Finally, the high-resolution profile α^E is derived using Eqn. 3 and downsampled to the ECMWF impact parameter grid $p_i^E \equiv n^E(z_i) \cdot (z_i - h_G + r_E)$ by a log-linear fit of α^E within each of the 91 impact parameter bins

$$[p_i^E - \delta p_i^-, p_i^E + \delta p_i^+] \qquad j = 1, \ldots, 91$$

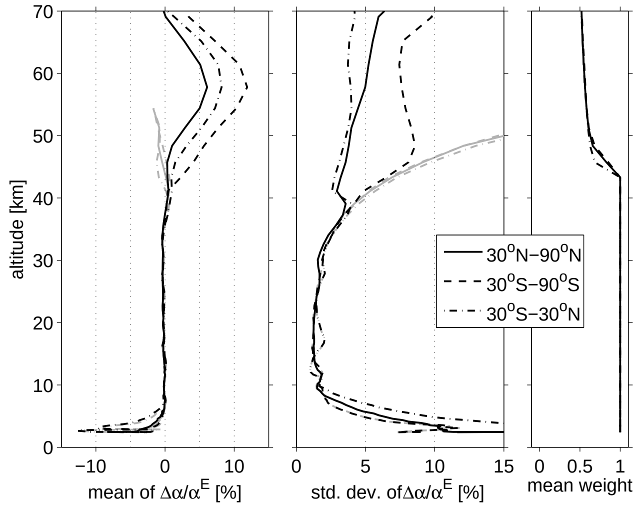

Figure 2: Comparison of 15,327 IGOR (TerraSAR-X) bending angle profiles with collocated ECMWF analysis results. The measurement period is 24 July to 17 November 2008. Statistically optimized bending angles are plotted in black, grey lines mark the corresponding result for the non-optimized (raw) observation. The data is processed by GFZ's experimental processing system POCS-X using single differencing. Left: mean fractional bending angle error for three meridional zones, 90^{o}S–30^{o}S (dashed lines), 30^{o}S–30^{o}N (dashed-dotted), 30^{o}N–90^{o}N (solid). Center: standard deviation of fractional bending angle error. Right: mean value of the statistical optimization weight.

and evaluation of the fit function at p_i^E. Here, $(z_i - h_G + r_E)$ is the ray tangent radius, r_E denotes Earth's local curvature radius, h_G is the geoid height and

$$\delta p_i^+ \equiv \delta p_{i+1}^- \equiv \frac{1}{2}\left(p_{i+1}^E - p_i^E\right) .$$

In addition, we set $\delta p_1^- \equiv \delta p_1^+$ and $\delta p_{91}^+ \equiv \delta p_{91}^-$.

The result of the comparison between 15,327 IGOR (TerraSAR-X) GPSRO profiles and corresponding ECMWF data in terms of the fractional bending angle error as a function of ray height is shown in figure 2. The mean and standard deviation of $\Delta\alpha/\alpha^E \equiv (\alpha^{RO} - \alpha^E)/\alpha^E$, are plotted in the left and middle panel of figure 2 (black lines) for the three latitudinal bands 90^oS to 30^oS (4,418 profiles), 30^oS to 30^oN (5,705 profiles) and 30^oN to 90^oN (5,204 profiles). In addition, the corresponding result using the non-optimized instead of the statistically optimized bending angles are plotted up to ray heights of 55 km (grey lines). Above 55 km the (non-optimized) results exhibit strong fluctuations exceeding 100% (not shown). The right panel shows the averaged statistical optimization weight w_{SO} corresponding to the three subsets. w_{SO} gives the relative contribution of the observed to the statistically optimized bending angle α^{RO} (Sokolovskiy and Hunt, 1996; Hocke, 1997; Healy, 2001; Wickert et al., 2004). E.g. $w_{SO} = 0.7$ indicates that the a-priori profile, derived from the MSIS climatology (Hedin, 1991), contributes 30% to α^{RO} and the remaining 70% originate from the GPSRO observation.

The result of the comparison between 15,327 IGOR (TerraSAR-X) GPSRO profiles and corresponding ECMWF data in terms of the fractional refractivity error

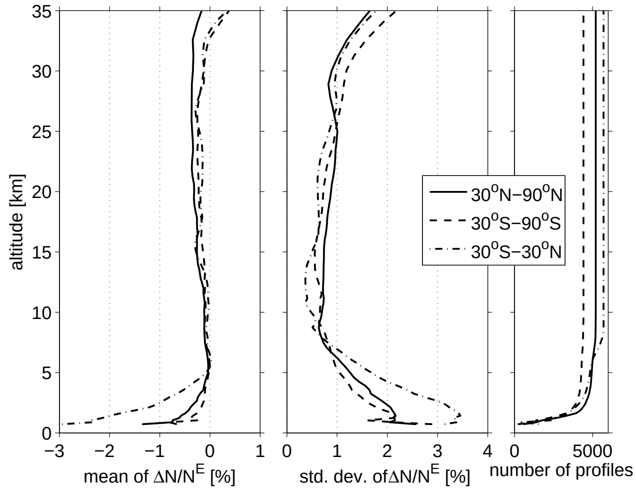

Figure 3: Statistical comparison of 15,327 IGOR (TerraSAR-X) refractivity profiles with collocated ECMWF analysis results. The observation period is 24 July to 17 November 2008. The data is processed by by GFZ's experimental processing system POCS-X using single differencing. Left: mean fractional refractivity error for three meridional zones, 90^{o}S-30^{o}S (dashed lines), 30^{o}S-30^{o}N (dashed-dotted), 30^{o}N-90^{o}N (solid). Center: standard deviation of the fractional refractivity error. Right: number of data points.

as a function of altitude is shown in figure 3. The mean and standard deviation of $\Delta N/N^E \equiv (N^{RO} - N^E)/N^E$, are plotted in the left and middle panel of figure 3 (black lines) for the three latitudinal bands. The right panel shows the number of refractivity observations as a function of altitude.

The biases of the mean fractional refractivity error at altitudes between 5 and 30 km varies between zero and -0.30%. Standard deviations decrease from about 1.4% at 5 km to about 0.6% at 10 km altitude, increase, however, significantly in the upper stratosphere. The strong negative bias of the mean fractional refractivity error at low latitudes and altitudes below 5 km is well known from earlier GPSRO missions (Ao et al., 2003; Xie et al., 2010) and most likely related to critical refraction at and within the tropical boundary layer. Recently, Sokolovskiy et al. (2010) describe a significant correlation between the lowest line-of-sight altitude and the mean fractional refractivity error in the lower troposphere. By adjusting the cut-off height for each individual occultation event they succeed in reducing the tropospheric bias to less than -1% for non-tropical and to about -2% for tropical observations (Sokolovskiy et al., 2010). We note that these advanced methods for an optimal adjustment of retrieval parameters are not implemented in GFZ's GPSRO processing systems.

For comparison, the corresponding mean and standard deviation of the fractional refractivity error profiles from GRACE-A observations are plotted in figure 4 (Beyerle et al., 2005; Wickert et al., 2009). The data set, containing 15,159 GPSRO observations, was collected during the same period as the TerraSAR-X measurements (24 July to 17 November 2008) and processed by GFZ's operational processing system POCS (Wickert et al., 2009).

The comparison of both, IGOR (TerraSAR-X) and BlackJack (GRACE-A) data with

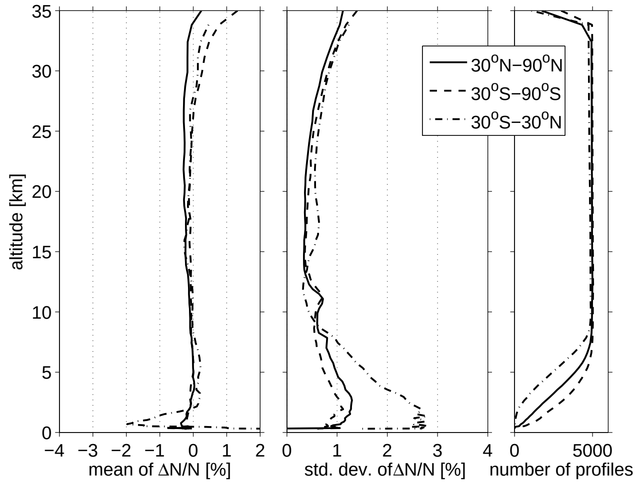

Figure 4: Same as figure 3 but for 15,159 GRACE-A GPSRO observations recorded during the same time period and processed by GFZ's operational processing system POCS.

ECMWF refractivities (figures 3 and 4) exposes a small increase in standard deviation at the tropical tropopause (about 16–18 km altitude). Most likely these features are related to inadequate ECMWF modelling of small scale structures at the tropical tropopause level. The occurrence of enhanced standard deviations is most prominent at the tropical tropopause level, though; in both data sets standard deviations decrease by about a factor of two when comparing refractivities at the tropopause and about 4 to 6 km below that altitude.

Both, the IGOR (TerraSAR-X) as well as the GRACE-A results exhibit a negative refractivity bias of about -0.2 to -0.3% in the upper troposphere and lower stratosphere. (left panels in figures 3 and 4). Whilst the observed refractivity bias might to some degree induced by ECMWF, we should also point out that N^{RO} is sensitive to the particular choice of filter parameters in a polynomial derivative filter which is used to smooth the excess Doppler profile. Assuming a tangent point vertical velocity of 2 km/s a filter of degree three and order 101 translates into a cut-off wavelength (-3 dB point) of about 3.33 km (see, e.g., Hamming, 1989; Beyerle and McDermid, 1999). In other words, the filter attenuates vertical wavelengths shorter that about 6.7 km by more than 50%. Reduction of the filter degree from three to two and a change of the filter order from 101 to 41 yields a cut-off wavelength of about 2.86 km. The corresponding refractivity error statistics are plotted in figure 5. The modified filter improves the average bias in the altitude region between 5 and 30 km by about a factor of two from -0.17% to -0.08%.

The main difference between the IGOR and BlackJack results in the lower troposphere is due to OL signal tracking implemented in IGOR (TerraSAR-X) and modified closed-loop ("fly-wheeling") tracking implemented in BlackJack (GRACE-A) (Ao et al., 2003; Beyerle et al., 2006). OL tracking significantly improves the data yield at altitudes below about 7 km, as is evident from the comparison of the observation number profiles (right panels in figures 3 and 4). The improvement in tropospheric penetration gained by OL tracking is quantitatively described in terms of the 50%-altitude $z_{50\%}$, which we define as the altitude at which the normalized number of ob-

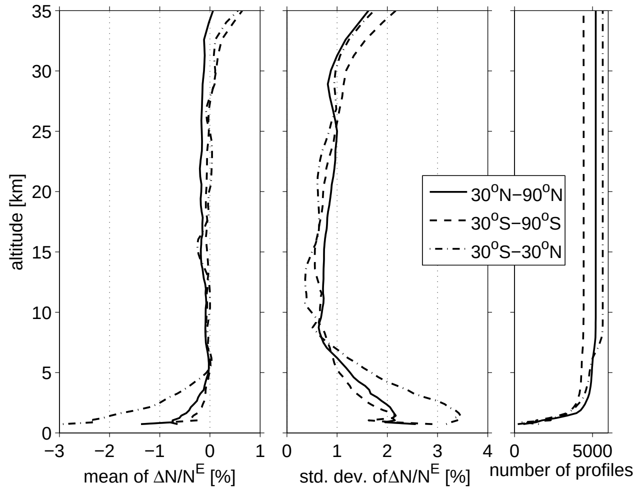

Figure 5: Same as figure 3, but derivative filter parameters reduced from degree three to two and filter order reduced from 101 to 41 (for details see text).

servations decreases to 50%. Specifically, the IGOR (TerraSAR-X) data set yields $z_{50\%} = 1.22$ km, 1.35 km and 1.23 km for the three latitude regions 30^oN to 90^oN, 30^oS to 30^oN and 90^oS to 30^oS. These depths are about 1.5 to 3.5 km lower than the corresponding 50%-altitudes derived from the BlackJack (GRACE-A) data set, which are $z_{50\%} = 3.22$ km, 5.00 km and 2.06 km for the same three latitudinal zones."

Specific Remarks:

Page 28824, Line 2:
GRAS seems to be missing here. ROSA could also be mentioned.

Fixed; the revised sentence reads: "Beginning with the proof-of-concept GPS/MET mission GPSRO instruments were placed on a number of spacecrafts, such as CHAMP, GRACE-A/B, SAC-C, Ørsted, the six-satellite COSMIC constellation, MetOp-A and OCEANSAT-2."

The following references are added to the revised manuscript:

Luntama, J.-P., Kirchengast, G., Borsche, M., Foelsche, U., Steiner, A., Healy, S., von Engeln, A., OClerigh, E., and Marquardt, C.: Prospects of the EPS GRAS Mission For Operational Atmospheric Applications, Bull. Am. Meteorol. Soc., 89, 18631875, doi:10.1175/2008BAMS2399.1, 2008.

and

Perona, G., Notarpietro, R., and Gabella, M.: GPS radio occultation on-board the OCEANSAT-2 mission: An Indian (ISRO) Italian (ASI) collaboration, Indian Journal of Radio Space Physics, 36, 386393, 2007.

Page 28826, Line 9:
You focus on the data recorded prior to this SW patch - is there any effect of this update on the data quality?

The relevant changes to the receiver firmware were related to the occultation manager (the number of satellites tracked in 50 Hz occultation mode at a given time are no longer restricted to one), the elimination of a memory leak and the implementation forward-looking occultations. A general effect on GPSRO data quality was not observed, though.

Page 28826, Line 25:
Recent work by Sergey shows that there is still signal at lower LSAs. Is this detectable on TerraSAR-X as well?

This type of analysis has not been performed with the TerraSAR-X data set. The lower LSA value was kept fixed at -120 km by the corresponding IGOR command; the actual value, however, varied between -80 to -150 km as illustrated in the manuscript's figure 2. Given that the IGOR aboard TerraSAR-X is almost identical in terms of hardware and firmware, we expected, that Sergey's results could be re-produced with the TerraSAR-X data set.

How does the receiver decide where an occultation ends?

The IGOR control command parameter 'RegionBottom' affects the lower LSA value. 'RegionBottom' doesn't determine the lower LSA value completely as is evident from the finite width of the histogram distribution shown in the manuscript's figure 2 (dark grey bars). Apparently other criteria contribute to the cut-off LSA value as well. Unfortunately, the IGOR user documentation does not provide more detail on the nature of these additional criteria.

Page 28831, Line 11 / Table 1:
What is the main reason for loosing so many occultations? It seems similar to COSMIC statistics, but not to GRAS ones.

The main reason for the high percentage of dropped events is insufficient length (number of samples) of an occultation measurement. That problem was exacerbated by a data buffer problem in the TerraSAR-X data computer which handles the IGOR data stream. Under certain conditions individual data packets were lost causing a 1 second data gap in the high rate occultation data. For consistency, we decided to remove the affected measurements rather than implementing an interpolation scheme to bridge these measurement gaps. Furthermore, the second-largest fraction is due to missing navigation bit data. Missing navigation bits lead directly to a rejection of the corresponding occultation event since we do not employ internal navigation bit reconstruction.

We note, that both issues have been addressed in the meantime. The data buffer problem was solved by a software upload and the coverage of GFZ's navigation bit network has grown from about 75% at the time period discussed (fall 2008) here to more than 99% today (spring 2011).

Page 28831, Line 16 / Figure 4:
One could also deduce from this figure that CHAMP is capable of tracking occultations even with SNRs around 200, while TerraSAR-X does not see any with this low SNRs. Now this could be cause by TerraSAR-X generally seeing higher SNRs of an occultation, but what about at very high azimuth angles, where theoretically these occultations could be tracked but none are found (for both instruments actually)? Is TerraSAR-X

driven by the antenna performance (thus azimuth angles higher than 55 Degrees are never observed) while CHAMP is driven by tracking performance?

TerraSAR-X does not observe events with SNR as low as 200 V/V since the azimuthal cut-off angle is set to 55° (the same value as used on CHAMP).

Page 28832, Line 11:
Is there always an increase when using the reference link? Isn't this the same data that is also used for POD, so it is anyway tracked, or is the POD tracking at lower frequency?

Yes, there is always an increase when a reference satellite is tracked since in GPS-RO mode data is sampled at 50 Hz; POD mode data (phase and pseudorange data) are sampled at 0.1 Hz.

Page 28833, Line 9, Figure 5:
I was naively assuming that the 30 s clock solution would introduce deviations the further one is away from the 30 s sampling point. This does not seem to be the case, rather a general degradation higher up is observed. Is there any further explanation for this? Is the 30s solution just so bad that it cannot be used at all?

It is correct that the difference between single- and zero-differencing excess phase (almost) vanishes at the 30 s sampling points. However, the deviations between single- and zero-differencing excess phases cause corresponding refractivity errors which are strongly height-dependent: in the stratosphere the sensitivity is higher compared to the lower troposphere. I.e., a certain excess phase error causes a much larger fractional refractivity error at 30 km than at 10 km altitude.

Page 28836, Line 23:
I probably don't understand enough of these NCO refractivities, but I would assume that there will generally be a bias between the N^{NCO} and the true N when the underlying model / climatology steering the NCO has a bias with respect to the true atmospheric state. And this will show up more when extreme conditions are found (low SNRs), which will not be near a climatological mean.

Yes, that correctly describes our hypothesis. If this hypothesis turns out to be true, i.e. if the NCO Doppler model maps through to the retrieved profiles at low SNR, then GPSRO-derived climatologies may depend on receiver-specific firmware implementations. One possible solution to address this issue is the addition of another open-loop tracking channel operating a slightly different NCO Doppler frequency (page 28837, lines 10-15).

Page 28837, Validation:
Would be nice to see also bending angles, up to some 50 or 60 km.

See our answer to the general comment above.

Page 28838, Line 3:
These 29 occultations were removed in a quality control procedure? They must have an ECMWF refractivity profile as long as they have a latitude, longitude, time entry.

The 29 occultation events were removed because in the (independently created) ECMWF data set the corresponding events were not considered. For the revised version the ECMWF profile extraction process was repeated with the current GPS-RO data including all observations.

References

Ao, C. O., Meehan, T. K., Hajj, G. A., Mannucci, A. J., and Beyerle, G.: Lower-Troposphere Refractivity Bias in GPS Occultation Retrievals, J. Geophys. Res., 108, 4577, doi:10.1029/2002JD003216, 2003.

Beyerle, G. and McDermid, I. S.: Altitude range resolution of differential absorption lidar ozone profiles, Appl. Opt., 38, 924–927, doi:10.1364/AO.38.000924, 1999.

Beyerle, G., Wickert, J., Schmidt, T., and Reigber, C.: GPS radio occultation with GRACE: Atmospheric profiling utilizing the zero difference technique, Geophys. Res. Lett., 32, L13806, doi:10.1029/2005GL023109, 2005.

Beyerle, G., Schmidt, T., Wickert, J., Heise, S., Rothacher, M., König-Langlo, G., and Lauritsen, K. B.: Observations and simulations of receiver-induced refractivity biases in GPS radio occultation, J. Geophys. Res., 111, D12101, doi:10.1029/2005JD006673, 2006.

Fjeldbo, G., Kliore, A. J., and Eshleman, V. R.: The neutral atmosphere of Venus as studied with the Mariner V radio occultation experiments, Astron. J., 76, 123–140, 1971.

Hamming, R. W.: Digital filters, Prentice Hall, Englewood Cliffs, NJ, 1989.

Healy, S. B.: Smoothing radio occultation data bending angles above 40 km, Ann. Geophysicae, 19, 459–468, 2001.

Hedin, A. E.: Extension of the MSIS thermosphere model into the middle and lower atmosphere, J. Geophys. Res., 96, 1159–1172, 1991.

Hocke, K.: Inversion of GPS meteorology data, Ann. Geophysicae, 15, 443–450, 1997.

Sokolovskiy, S. and Hunt, D.: Statistical optimization approach for GPS/MET data inversions, in: URSI GPS/MET workshop, Union Radio Sci. Int., 1996.

Sokolovskiy, S., Rocken, C., Schreiner, W., and Hunt, D.: On the uncertainty of radio occultation inversions in the lower troposphere, J. Geophys. Res., 115, D22111, doi:10.1029/2010JD014058, 2010.

Wickert, J., Schmidt, T., Beyerle, G., König, R., Reigber, C., and Jakowski, N.: The radio occultation experiment aboard CHAMP: Operational data analysis and validation of atmospheric profiles, J. Meteorol. Soc. Jpn., 82, 381–395, 2004.

Wickert, J., Michalak, G., Schmidt, T., Beyerle, G., Cheng, C., Healy, S., Heise, S., Huang, C., Jakowski, N., Köhler, W., Mayer, C., Offiler, D., Ozawa, E., Pavelyev, A., Rothacher, M., Tapley, B., and Arras, C.: GPS radio occultation: Results from CHAMP, GRACE and FORMOSAT-3/COSMIC, Terrestrial, Atmospheric and Oceanic Sciences, 20, 35–50, doi:10.3319/TAO.2007.12.26.01(F3C), 2009.

Xie, F., Wu, D. L., Ao, C. O., Kursinski, E. R., Mannucci, A. J., and Syndergaard, S.: Super-refraction effects on GPS radio occultation refractivity in marine boundary layers, Geophys. Res. Lett., 35, L11805, doi:10.1029/2010GL043299, 2010.